A&A 518, L110 (2010)
DOI: 10.1051/0004-6361/201014576
© ESO 2010

Astronomy & Astrophysics
Special feature

Herschel: the first science highlights

Letter to the Editor

Interstellar OH^+, H_2O^+ and H_3O^+ along the sight-line to G10.6–0.4⋆,⋆⋆

M. Gerin[1], M. De Luca[1], J. Black[2], J. R. Goicoechea[3], E. Herbst[4], D. A. Neufeld[5], E. Falgarone[1], B. Godard[1,8], J. C. Pearson[6], D. C. Lis[7], T. G. Phillips[7], T. A. Bell[7], P. Sonnentrucker[5], F. Boulanger[8], J. Cernicharo[3], A. Coutens[12,13], E. Dartois[8], P. Encrenaz[1], T. Giesen[9], P. F. Goldsmith[6], H. Gupta[6], C. Gry[10], P. Hennebelle[1], P. Hily-Blant[11], C. Joblin[12,13], M. Kazmierczak[15], R. Kolos[14], J. Krelowski[15], J. Martin-Pintado[3], R. Monje[7], B. Mookerjea[16], M. Perault[1], C. Persson[2], R. Plume[17], P. B. Rimmer[4], M. Salez[1], M. Schmidt[18], J. Stutzki[9], D. Teyssier[19], C. Vastel[12,13], S. Yu[6], A. Contursi[20], K. Menten[21], T. Geballe[22], S. Schlemmer[9], R. Shipman[23], A. G. G. M. Tielens[24], S. Philipp-May[21,25], A. Cros[12,13], J. Zmuidzinas[7], L. A. Samoska[6], K. Klein[25], and A. Lorenzani[27]

(Affiliations are available in the online edition)

Received 30 March 2010 / Accepted 30 April 2010

ABSTRACT

We report the detection of absorption lines by the reactive ions OH^+, $H_2O^+$and H_3O^+ along the line of sight to the submillimeter continuum source G10.6−0.4 (W31C). We used the *Herschel* HIFI instrument in dual beam switch mode to observe the ground state rotational transitions of OH^+ at 971 GHz, H_2O^+ at 1115 and 607 GHz, and H_3O^+ at 984 GHz. The resultant spectra show deep absorption over a broad velocity range that originates in the interstellar matter along the line of sight to G10.6−0.4 as well as in the molecular gas directly associated with that source. The OH^+ spectrum reaches saturation over most velocities corresponding to the foreground gas, while the opacity of the H_2O^+ lines remains lower than 1 in the same velocity range, and the H_3O^+line shows only weak absorption. For LSR velocities between 7 and 50 km s^{-1} we estimate total column densities of $N(OH^+) \geq 2.5 \times 10^{14}$ cm^{-2}, $N(H_2O^+) \sim 6 \times 10^{13}$ cm^{-2} and $N(H_3O^+) \sim 4.0 \times 10^{13}$ cm^{-2}. These detections confirm the role of O^+ and OH^+ in initiating the oxygen chemistry in diffuse molecular gas and strengthen our understanding of the gas phase production of water. The high ratio of the OH^+ by the H_2O^+ column density implies that these species predominantly trace low-density gas with a small fraction of hydrogen in molecular form.

Key words. ISM: general – ISM: molecules – ISM: clouds

1. Introduction

Oxygen chemistry in the interstellar medium is initiated by cosmic-ray or X-ray ionization of hydrogen. The resulting H^+ and H_3^+ transfer their charge to form the O^+ and OH^+ ions, both of which react rapidly with H_2 molecules. Subsequent H-atom abstraction reactions proceed to the terminal ion H_3O^+ with high efficiency, unless the electron fraction is unusually high. H_3O^+ does not react with H_2 or any other abundant neutral species, but is destroyed by dissociative recombination with electrons. Recombination produces O, OH, and H_2O. This sequence is the main gas-phase chemical route to water in the interstellar medium. Until now, this classical scheme of the oxygen chemistry (Herbst & Klemperer 1973) has been tested mainly through observations of OH and H_2O, whose abundances are affected by many other processes as well, and by a few observations of H_3O^+. With the HIFI instrument on the *Herschel* satellite it is now possible to observe the strongest transitions of light hydrides, including the reactive molecular ions OH^+ and H_2O^+ that are thought to play crucial intermediate roles in the formation of OH and H_2O.

Previous attempts to observe interstellar H_2O^+ and OH^+ from optical spectroscopy are very limited. Smith et al. (1984) report an upper limit of 10^{12} cm^{-2} for H_2O^+ based on optical absorption spectroscopy. No observation of the OH^+ transition at 358.4 nm has been reported until very recently (Krelowski et al., private communication). Submillimeter telescopes have been more successful in detecting these ions. With the Atacama Pathfinder EXperiment (APEX) telescope Wyrowski et al. (2010) detected two hyperfine-structure components of the OH^+ $N = 1-0$ $J = 0-1$ transition near 909.2 GHz towards the strong continuum source Sgr B2(M) and concluded that OH^+ plays a major role in the chemistry of the diffuse molecular gas. Using HIFI on *Herschel*, Ossenkopf et al. (2010) report the detection of o-H_2O^+ absorption in the three massive star-forming regions NGC 6334, Sgr B2, and DR 21.

We present observations toward the massive star-forming region G10.6−0.4 (W 31C) located at $RA = 18^h10^m28.70^s$, $Dec = -19°55'50$ s (J2000). The submillimeter-wave continuum emission is associated with a cluster of ultra-compact H II regions located in the so-called "30 km s^{-1} arm" at a kinematic distance of 4.8 kpc (Fish et al. 2003; Corbel & Eikenberry 2004). The molecular cloud surrounding the star-forming complex shows evidence of continuing accretion onto the embedded stars (Keto & Wood 2006; Sollins & Ho 2005). As discussed by Neufeld et al. (2010), line absorption by foreground gas has been detected from [OI] (Keene et al. 1999), $^{13}CH^+$ (Falgarone et al. 2005), HCO^+, HCN, HNC, CN (Godard et al. 2010), and atomic hydrogen (Fish et al. 2003). While the gas associated directly with G10.6−0.4 is detected in the velocity range −5 to +5 km s^{-1}, the

⋆ *Herschel* is an ESA space observatory with science instruments provided by European-led Principal Investigator consortia and with important particiation from NASA.

⋆⋆ Figure 2 is only available in electronic form at http://www.aanda.org

Table 1. Transition spectroscopic parameters.

Transition	Frequency MHz	Error MHz	E_l cm^{-1}	A 10^{-2} s^{-1}	Ref.
$OH^+ N = 1 - 0$					
$2, 5/2 - 1, 3/2$	971803.8	1.5	0.0	1.82	1
$2, 3/2 - 1, 1/2$	971805.3	1.5	0.0	1.52	1
$2, 3/2 - 1, 3/2$	971919.2	1.0	0.0	0.30	1
o-$H_2O^+ 1_{1,1} - 0_{0,0}$					
$3/2, 3/2 - 1/2, 1/2$	1115122.0	10	0.0	1.71	2
$3/2, 1/2 - 1/2, 1/2$	1115158.0	10	0.0	2.75	2
$3/2, 5/2 - 1/2, 3/2$	1115175.8	10	0.0	3.10	2
$3/2, 3/2 - 1/2, 3/2$	1115235.6	10	0.0	1.39	2
$3/2, 1/2 - 1/2, 3/2$	1115271.6	10	0.0	0.35	2
p-$H_2O^+ 1_{1,0} - 1_{0,1}$					
$3/2, 3/2 - 3/2, 3/2$	607207.0	20	20.9	0.60	2
H_3O^+					
$0_0^- - 1_0^+$	984711.9	0.3	5.1	2.3	3

References. 1, Müller et al. (2005) & CDMS; 2, Strahan et al. (1986), Ossenkopf et al. (2010); 3 Yu et al. (2009) & JPL catalog.

foreground gas along the line of sight is confined to the velocity interval from ~5 to 45 km s^{-1}.

2. Spectroscopy

Table 1 summarizes the spectroscopic parameters used for the searched transitions. The OH^+ ion has a $^3\Sigma^-$ electronic ground state. We used the data from Beekoy et al. (1985) with reported uncertainties for the line frequencies better than about 1.5 MHz. Müller et al. (2005) have published a global fit using these data which is available in the Cologne Data base for Molecular Spectroscopy (CDMS). The ground state dipole moment obtained from theoretical calculations is 2.3 D (Werner et al. 1983; Cheng et al. 2007).

The spectroscopic properties of H_2O^+ are extensively discussed in the accompanying letter (Ossenkopf et al. 2010). Its dipole moment is very similar to that of OH^+, as recently calculated by Wu et al. (2004), who found the ground state dipole moment to be 0.933, mistakenly printed in atomic units for a value of 2.370 Debye. This molecular ion has ortho and para symmetry states, which have the opposite parity to the water vapor molecule, i.e. the lowest state is the ortho state. Therefore the ortho/para ratio should be at least 3:1.

H_3O^+ has been the subject of many spectroscopic investigations, because for the frequency of the inversion transition of this molecular ion is comparable to the rotational constant. The most recent analysis has been presented by Yu et al. (2009) and is available in the JPL spectral line catalog. We observed the lowest transition from the E symmetry state, which is ~5 cm^{-1} above the ground state.

3. Observations

The observations were carried out by the HIFI instrument on board *Herschel* (Pilbratt et al. 2010; de Graauw et al. 2010), in the double beam switching (DBS) mode. We used the wide band spectrometer (WBS) with 4 GHz bandwidth and 1.1 MHz effective spectral resolution. To help separate the signals from the lower and upper sidebands, three integrations were carried out at each frequency, with the local oscillator (LO) shifted by 15 km s^{-1}.

The data were first processed with HIPE Ott et al. (2010) and subsequently exported to CLASS. We checked that the target lines did not suffer from any contamination by lines from the other sideband and that the absorption features were not contaminated by emission in the reference beam. The two polarizations excellently agree – the continuum levels agree to better than 10% – except for the OH^+ line, where the V polarization shows ripples and has therefore not been used in the present analysis. We combined the data from the three LO tunings and the two polarizations to obtain the average spectra shown in Fig. 1. For double-side band mixers with equal sideband gains, fully saturated lines are expected to absorb only half of the continuum signal. This expectation is borne out in the present data. While the OH^+ line is clearly saturated, both H_2O^+lines show moderate absorption, while the H_3O^+ line only shows weak absorption.

4. Results

To understand the structure of the absorption profiles and derive column densities of the reactive ions, we normalized the spectra by the SSB continuum intensities. We constructed empirical models of the line profiles by combining multiple velocity components, defined by their central velocity, line width, and opacity. The predicted spectrum was then computed by combining the contributions of the hyperfine components (3 for OH^+ and 5 for H_2O^+ as listed in Table 1) to the overall line profile. We show in Fig. 1 spectra normalized by the continuum intensities, with the synthetic spectra superimposed. Table 2 lists the model parameters.

Although we obtained good fits of the OH^+ and H_2O^+ profiles, it is likely that the solution is not unique because the number of velocity components is not well constrained. The OH^+ ground state lines are known with a good accuracy of ~1.5 MHz. Velocities obtained by the empirical model agree well with the velocities where deep HCO^+(1-0) (Keene et al. 1999; Godard et al. 2010), p-H_2O and HF (Neufeld et al. 2010) and HI Fish et al. (2003) absorptions are detected. It is remarkable that one of the strongest OH^+ absorption features at $V_{LSR} \sim 7$ km s^{-1} coincides with a strong dip in the HI profile that has no counterpart in CO emission Falgarone et al. (2005). Overall, the velocities of the OH^+ and H_2O^+ velocity components agree well. Although the lines are detected in absorption, given the similarity of their Local Standard of Rest (LSR) velocities with the rest velocity of G10.6−0.4, it is likely that the most blueshifted velocity components are associated with the G10.6−0.4 molecular complex.

Below we discuss the column densities and abundances of OH^+, H_2O^+, and H_3O^+ in the foreground interstellar gas, with LSR velocities higher than 5 km s^{-1}. Neufeld et al. (2010) discuss the total column density of this material and obtain a column density of hydrogen in all forms of $N_H \sim 2.7 \times 10^{22}$ cm^{-2}. This figure is consistent with the lower limit derived from the oxygen column density measured with ISO, 5×10^{18} cm^{-2} (Keene et al. 1999), which gives $N_H > 1.7 \times 10^{22}$ cm^{-2} using O/H = 3×10^{-4}. For this line of sight the estimated atomic hydrogen column density is at most N(HI) = 1.2×10^{22} cm^{-2} (Godard et al. 2010), hence the average fraction of hydrogen in molecular form is $f(H_2) \sim 0.6$, with significant variations among the velocity components.

The total OH^+ and H_2O^+ column densities were obtained by summing the contributions of the velocity components with centroids larger than 7 kms^{-1}. We derive $N(OH^+) \geq 2.5 \times 10^{14}$ cm^{-2} and N(o-H_2O^+) = 4.4×10^{13} cm^{-2}. Although the absorption from the p-H_2O^+ line at 607 GHz is blended with emission from $H^{13}CO^+$(6-5) at 607175 MHz, weak absorption is clearly detected in the velocity range of the foreground gas along the line of sight to G10.6−0.4. The integrated opacity for the LSR velocity range 20 to 45 km s^{-1} is $\int \tau dv = 2$ km s^{-1}, corresponding to a total column density of $\sim 1 \times 10^{13}$ cm^{-2}. This figure is obtained for a limited velocity range, and should therefore be considered a lower limit. Given the uncertainties, the data

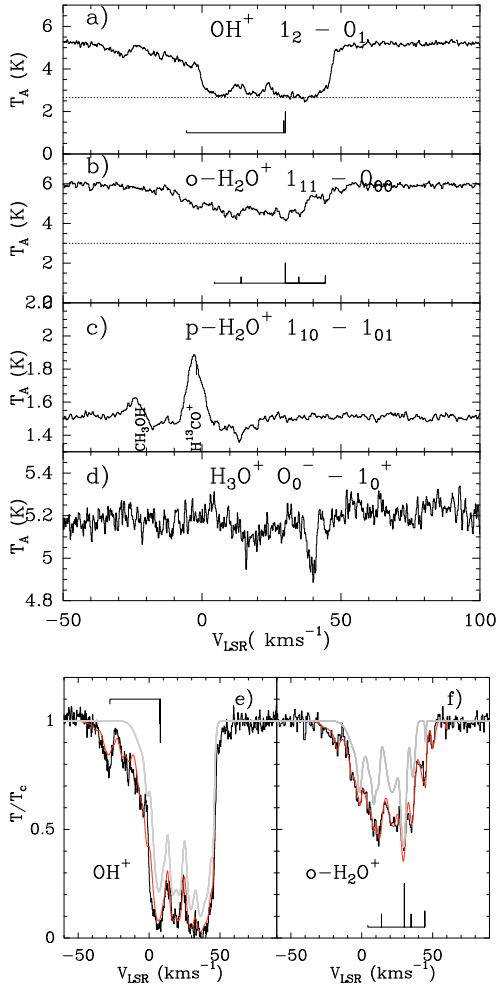

Fig. 1. HIFI spectra of **a)** OH^+; **b)** o-H_2O^+; **c)** p-H_2O^+ and (d) H_3O^+. The hyperfine structure of the OH^+ and o-H_2O^+ lines (see Table 1) is indicated. In both cases, the velocity scale corresponds to the rest frequency of the strongest hyperfine component. In panel c), the velocity scale refers to the frequency of the $H^{13}CO^+$ (6-5) line at 607174.65 MHz. Panel d) uses the frequency of 984711.907 MHz. Panels e) and f) show overlays with the synthetic spectra constructed with the empirical models detailed in Table 2. Grey curves show the profile of the strongest hyperfine component.

are consistent with an o/p ratio of 3 for H_2O^+, as expected from the spin statistics. The total column density of H_2O^+ is therefore $N(H_2O^+)$ ~6×10^{13} cm^{-2} and the abundance ratio $N(OH^+)/N(H_2O^+) \geq 4$. Using the total gas column density , we conclude that OH^+ and H_2O^+ reach fractional abundances, of $N(OH^+)/N_H \geq \times 10^{-8}$ and $N(H_2O^+)/N_H \sim 2 \times 10^{-9}$.

The H_3O^+spectrum shows a sharp feature with strongest absorption at $V_{LSR} \sim 40$ km s^{-1}and a broad component centered at $V_{LSR} \sim 20$ km s^{-1}. This velocity structure is more similar to the HF or p-H_2O spectra than the OH^+ and H_2O^+ velocity structure, confirming that these molecular ions trace different physical conditions. We derived the H_3O^+ column density of the foreground gas for all velocity components. Assuming an excitation temperature of 5 K, appropriate for the conditions of the gas in the inner galaxy, we derive $N(H_3O^+)$ ~4×10^{13} cm^{-2} for the LSR velocity range 7–45 km s^{-1}. Therefore N(OH^+)/N(H_3O^+) > 6 and N(H_2O^+)/N(H_3O^+) ~1.5. These numbers represent the average for all velocity components but, given the different velocity structure of H_3O^+ and OH^+, the column density ratio for individual velocity components can significantly differ from the average value.

Table 2. Empirical models used to analyze the OH^+ and H_2O^+spectra.

	OH^+			H_2O^+		
V_{LSR}	Δ_V	τ	N	Δ_V	τ	N
km s^{-1}	km s^{-1}		10^{13} cm^{-2}	km s^{-1}		10^{12} cm^{-2}
–1.0	14.0	0.2	1.3	14.0	0.2	12
–1.5	3.0	0.2	0.3	3.0	0.2	2.5
5.5	6.0	1.0	2.8	3.0	0.15	1.9
8.5	5.0	0.8	1.9	3	0.4	5.0
11.5	3.0	0.5	0.7	3.0	0.3	3.8
16.5	5.0	1.5	3.5			
21.5	5.0	1.5	3.5	10.0	0.4	1.7
29.5	6.0	2.0	5.6	4.0	0.8	1.3
36.0	5.0	2.0	4.7	3.5	0.3	4.4
41.0	6.0	1.5	4.2			
45.0	2.0	0.5	0.5	1.0	0.1	0.4

Notes. The OH^+ and H_2O^+ parameters refer to the frequency of the strongest hyperfine component (cf. Table 1).

5. Chemistry

5.1. PDR models

In order to model the OH^+ and H_2O^+ chemistry in diffuse clouds, we used the Meudon PDR code[1], a photochemical model of a plane parallel and stationary PDR (Le Petit et al. 2006; Goicoechea & Le Bourlot 2007). We present models for a representative cloud of $A_V = 1$ mag illuminated from both sides. Although the total extinction along this line of sight is ~14 mag (Corbel & Eikenberry 2004; Neufeld et al. 2010), the line profile clearly shows multiple velocity components, revealing interstellar clouds along the line of sight. As discussed by Godard et al. (2010), each of these clouds has low to moderate extinctions, corresponding to diffuse or transluscent matter.

The Meudon PDR code computes the gas temperature gradient by solving the thermal balance (see Le Petit et al. 2006). Our pure gas-phase chemical network is based on a modified version of the Ohio State University (OSU) gas-phase network updated for photochemical studies. The extinction of UV and visible radiation is computed using a dust grain size distribution following a power-law (Mathis et al. 1977). The adopted oxygen and carbon elemental abundances are 3.02×10^{-4} and 1.38×10^{-4}, respectively. As a starting point we used an ionization rate (of H) due to cosmic rays of $\zeta_H = 2.3 \times 10^{-17}$ s^{-1}.

The oxygen chemistry starts with the $O(^3P_J) + H^+ \rightarrow O^+(^4S) + H$ charge transfer process, where reaction rates are sensitive to the oxygen fine-structure level populations (Stancil et al. 1999, and references therein). Indeed the charge transfer proceeds quickly when the $O(^3P_1)$ level ($\Delta E_{12}/k = 228$ K) is significantly populated, but it can be a slow proceess in cold gas where only the $O(^3P_2)$ ground-state level is populated (Spirko et al. 2003). As listed in Table 3, OH^+ is formed by $O^+ + H_2$ with additional contribution from OH photoionization at the cloud edges, and by $O + H_3^+$. Therefore, the OH^+ abundance may be sensitive to gas temperature, far ultraviolet (FUV) radiation field and ζ_H.

In order to investigate the possible sources of the high OH^+/H_2O^+ abundance ratio, Fig. 2 shows photochemical models for different densities, and radiation fields (thus different gas temperatures). High OH^+/H_2O^+ abundance ratios are found in the warm gas at low extinction, where the fraction of hydrogen in molecular form is significantly smaller than 1. As a limited set reactions need to be considered we built a simplified analytical model based on the network listed in Table 3, and find

$$n(OH^+)/n(H_2O^+) = (k_2/k_1) + (k_3/k_1)[n(e^-)/n(H_2)] \quad (1)$$

[1] See http://pdr.obspm.fr/PDRcode.html

Table 3. Main chemical reactions.

Number	Reaction	Rate ($cm^{-3}s^{-1}$)
1	$OH^+ + H_2 \rightarrow H_2O^+ + H$	$k_1 = 1.01 \times 10^{-9}$
2	$H_2O^+ + H_2 \rightarrow H_3O^+ + H$	$k_2 = 6.4 \times 10^{-10}$
3	$H_2O^+ + e^- \rightarrow$ products	$k_3 = 4.3 \times 10^{-7}(T/300\,K)^{-0.5}$
4	$H_3O^+ + e^- \rightarrow$ products	$k_4 = 4.3 \times 10^{-7}(T/300\,K)^{-0.5}$
5	$OH^+ + e^- \rightarrow$ products	$k_5 = 3.75 \times 10^{-8}(T/300\,K)^{-0.5}$

$$= 0.64 + 430 \times (T/300)^{-0.5} \times [n(e^-)/n(H_2)]. \quad (2)$$

Using $f(H_2) = 2n(H_2)/(n(H) + 2n(H_2)) = 2n(H_2)/n_H)$ and assuming that all carbon is ionised ($n(e^-) = n_C = 1.4 \times 10^{-4} n_H$) Eq. (2) leads to $n(OH^+)/n(H_2O^+) = 0.64 + 0.12 \times (T/300)^{-0.5}/f(H_2)$. The data suggest that $N(OH^+)/N(H_2O^+) > 4$, implying that $f(H_2) < 0.06$ at $T = 100$ K, an appropriate temperature for diffuse gas in the molecular ring. Equation (2) determined for each Av in the model is shown as green lines in Fig. 2. It fits the modeled abundance perfectly, demonstrating that the main ingredients have been captured by this simple model. Note that the reactions were studied in the laboratory and their rates are known with a good accuracy.

5.2. The role of cosmic rays

Like H_3^+ (Indriolo et al. 2007), OH^+ and H_2O^+ can be used to trace the cosmic ray ionization rate for H atoms ζ_H. In the moderately warm gas where they are produced, the charge exchange reaction is rapid. Then, every cosmic ray ionization of H can lead to O^+ and we can use the measured OH^+ abundance to set limits on ζ_H. In addition to the reaction with H_2, OH^+ is destroyed in dissociative recombination reactions with electrons. This implies $\zeta_H > X(OH^+)x(e^-)n(H)k_5$, $\zeta_H > 9.2 \times 10^{-12} \times n(OH^+)$ at $T = 100$ K.

The lower limit on the OH^+ abundance in the atomic gas is $n(OH^+)/n(H) > 2 \times 10^{-8}$, which places a robust lower limit of $\zeta_H > 1.8 \times 10^{-19} n(H)$. This lower limit is very conservative: depending on the conditions in the absorbing material, higher values of ζ_H may prove necessary to account for the observed column densities of OH^+ and H_2O^+. The H_3^+ observations of diffuse interstellar clouds point toward an enhanced ionization rate at low extinction. In a future analysis we will consider how OH^+ and H_2O^+ can provide additional constraints upon ζ_H.

5.3. The role of turbulence

In the warm chemistry driven by intermittent turbulent dissipation (Godard et al. 2009), the production of OH^+ and H_2O^+ is enhanced compared to UV-driven chemistry, with an efficiency depending only on the turbulent dissipation rate, ϵ. For $\epsilon = 2 \times 10^{-24}$ ergcm^{-3}s^{-1}, ten times higher than the average Galactic value appropriate for the inner Galaxy, the TDR model predicts $N(CH^+) = 4.3 \times 10^{13}$ cm^{-3}, $N(OH^+) = 2 \times 10^{12}$ cm^{-2} and $N(H_2O^+) = 2.2 \times 10^{12}$ cm^{-2} per magnitude of gas of density $n_H = 50$ cm^{-3}. The ratios between these three species weakly depend on ϵ. With the observed CH^+ column density, 6.7×10^{14} cm^{-2} , derived from $^{13}CH^+$ (Falgarone et al. 2005)[2], we therefore expect the following contributions of the TDR chemistry in that line of sight: $N(OH^+) = 3.1 \times 10^{13}$ cm^{-2}, and $N(H_2O^+) = 3.4 \times 10^{13}$ cm^{-2}. The OH^+ column is well below the observed value, while that of H_2O^+ is interestingly close.

6. Conclusion

The detection of interstellar OH^+, H_2O^+, and H_3O^+provides a strong support to our understanding of the gas phase oxygen chemistry, in particular the gas phase route to water vapor. The combined analysis of the OH^+ and H_2O^+ ground state spectra has shown that they mostly reside in warmish atomic gas where they are produced in a reaction sequence initiated by atomic H ionization followed by rapid reaction with traces of H_2. Their abundances and abundance ratio can be used to constrain the fraction of hydrogen in molecular form, and to set a lower limit for the cosmic ray ionization in the diffuse gas, where few other diagnostics are applicable. As these reactive molecular ions can be observed from space with the *Herschel* Space Observatory, and in exceptional conditions from the ground, these preliminary conclusions should be verified by more extensive observations. It is also expected that strong features from both OH^+ and H_2O^+ will be detected in the spectra of distant galaxies, where elevated fluxes of ionizing radiation are produced by active nuclei and intense star-formation activity.

Acknowledgements. HIFI has been designed and built by a consortium of institutes and university departments from across Europe, Canada and the United States under the leadership of SRON, Netherlands Institute for Space Research, Groningen, The Netherlands, and with major contributions from Germany, France and the US. Consortium members are: Canada: CSA, U. Waterloo; France: CESR, LAB, LERMA, IRAM; Germany: KOSMA, MPIfR, MPS; Ireland: NUI Maynooth; Italy: ASI, IFSI-INAF, Osservatorio Astrofisico di Arcetri-INAF; Netherlands: SRON, TUD; Poland: CAMK, CBK; Spain: Observatorio Astronòmico Nacional (IGN), Centro de Astrobiologia; Sweden: Chalmers University of Technology – MC2, RSS & GARD, Onsala Space Observatory, Swedish National Space Board, Stockholm University – Stockholm Observatory; Switzerland: ETH Zurich, FHNW; USA: CalTech, JPL, NHSC. MG, EF, MDL acknowledge the support from CNES, and ANR through the SCHISM project (ANR-09-BLAN-231). M.S. acknowledges support from grant N203393334 (MNiSW).

References

Beekoy, J. P., Verhoeve, P., Meerts, W. L., et al. 1985, J. Chem. Phys., 82, 3868
Cheng, M., Brown, J. M., Rosmus, P., et al. 2007, Phys. Rev. A, 75, 012502
Corbel, S., & Eikenberry, S. S. 2004, A&A, 419, 191
Falgarone, E., Phillips, T. G., Pearson, J. C. 2005, ApJ, 634, L149
Fish, V. L., Reid, M. J., Wilner, D. J., et al. 2003, ApJ, 587, 701
Godard, B., Falgarone, E., Pineau, des Forêts, G. 2009, A&A, 495, 847
Godard, B., Falgarone, E., Gerin, M., et al. 2010, A&A, accepted
Goicoechea, J. R., & Le Bourlot, J. 2007, A&A, 467, 1
de Graauw, T., Helmich, F. P., Phillips, T. G., et al. 2010, A&A, 518, L6
Herbst, E., & Klemperer, W. 1973, ApJ, 185, 505
Indriolo, N., Geballe, T. R., Oka, T., & McCall, B. J. 2007, ApJ, 671, 1736
Keene, J., Lis, D. C., Phillips, T. G., et al. 1999, ESASP, 427, 687
Keto, E., & Wood, K. 2006, ApJ, 637, 85
Le Petit, F., Nehmé, C., Le Bourlot, J., & Roueff, E. 2006, ApJS, 164, 506
Mathis, J. S., Rumpl, W., & Nordsieck, K. H. 1977, ApJ, 217, 425
Müller, H. S. P., Schlöder, F., Stutzki, J., et al. 2005, Mol. Struct., 742, 215
Neufeld, D. A., Sonnentrucker, P., Phillips, T. G., et al. 2010, A&A, 518, L108
Ossenkopf, V., Müller, H. S. P., Lis, D. C., et al. 2010, A&A, 518, L111
Ott S., 2010, in Astronomical Data analysis Software and Systems XIX, ed. Y. Mizumoto, K. I. Morita, & M. Ohishi, ASP Conf. Ser., in press
Pilbratt, G., Riedinger, J. L., Passvogel, T., et al. 2010, A&A, 518, L1
Smith, W. H., Schempp, W. V., & Federman, S. R. 1984, ApJ, 277, 196
Sollins, P. K., & Ho, P. T. P. 2005, ApJ, 630, 987
Spirko, J. A., Zirbel, J. J., & Hickman, A. P. 2003, JPhB, 36, 1645
Stancil, P. C., Schultz, D. R., Kimura, M., et al. 1999, A&AS, 140, 225
Strahan, S. E., Müller, R. P., & Saykally, R. J. 1986, J. Chem. Phys., 85, 1252
Werner, H.-J., Rosmus, P., & Reinsch, E.-A. 1983, J. Chem. Phys., 79, 905
Wyrowski, F., Menten, K. M., Güsten, R., & Belloche, A. 2010, A&A, accepted [arkiv:1004.2627]
Wu, S., Chen, Y., Yang, X., et al. 2004, J. Mol. Spectrosc., 225, 96
Yu, S., Drouin, B. J., Pearson, J. C., & Pickett, H. M. 2009, ApJS, 180, 119

[2] In that paper it was underestimated by a factor 8 because of an unjustified approximation made in the derivation of the opacity.

Page 5 is available in the electronic edition of the journal at http://www.aanda.org

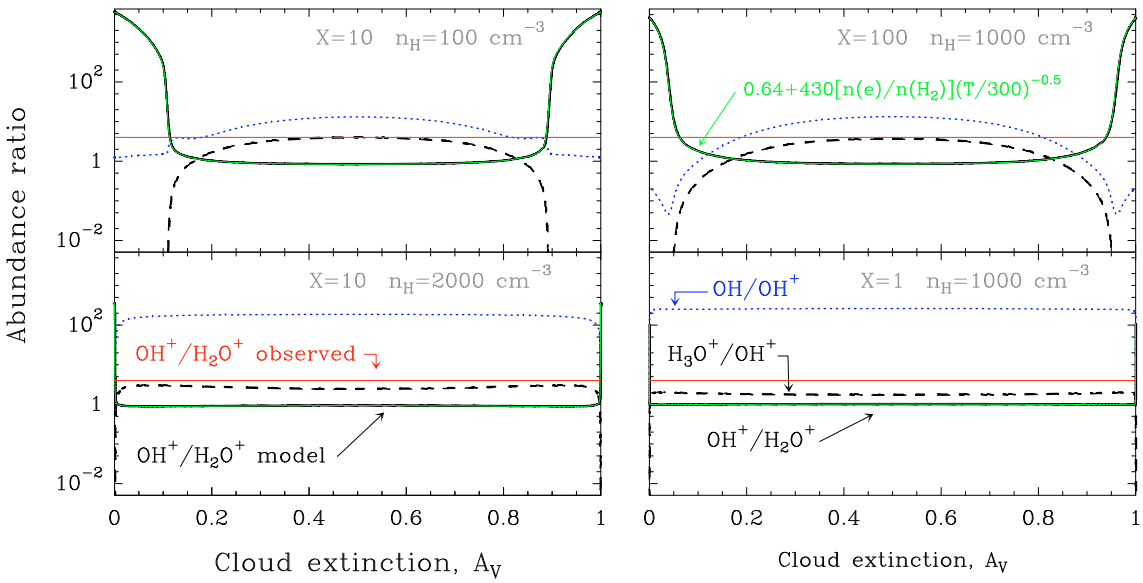

Fig. 2. Predictions of the Meudon-PDR model for a slab of A_v = 1 mag illuminated from both sides. The radiation field and gas density are given in each panel. Full lines: $n(OH^+)/n(H_2O^+)$, dotted lines: $n(OH)/n(OH^+)$, dashed lines: $n(H_3O^+)/n(OH^+)$. Equation (2) determined for each Av in the model is shown in green.

[1] LERMA, CNRS, Observatoire de Paris and ENS, France
e-mail: maryvonne.gerin@ens.fr
[2] Chalmers University of Technology, Göteborg, Sweden
[3] Centro de Astrobiología, CSIC-INTA, Madrid, Spain
[4] Depts. of Physics, Astronomy & Chemistry, Ohio State Univ., USA
[5] The Johns Hopkins University, Baltimore, MD 21218, USA
[6] JPL, California Institute of Technology, Pasadena, USA
[7] California Institute of Technology, Pasadena, CA 91125, USA
[8] Institut d'Astrophysique Spatiale (IAS), Orsay, France
[9] I. Physikalisches Institut, University of Cologne, Germany
[10] Laboratoire d'Astrophysique de Marseille (LAM), France
[11] Laboratoire d'Astrophysique de Grenoble, France
[12] Université de Toulouse; UPS; CESR; 9 avenue du colonel Roche, 31028 Toulouse Cedex 4, France
[13] CNRS; UMR5187; 31028 Toulouse, France
[14] Inst. of Physical Chemistry, Polish Academy of Sciences, Poland
[15] Nicolaus Copernicus University, Torún, Poland
[16] Tata Institute of Fundamental Research, Mumbai, India
[17] Dept. of Physics & Astronomy, University of Calgary, Canada
[18] European Space Astronomy Centre, ESA, Madrid, Spain
[19] MPI für Extraterrestrische Physik, Garching, Germany
[20] MPI für Radioastronomie, Bonn, Germany
[21] Gemini telescope, Hilo, Hawaii, USA
[22] Nicolaus Copernicus Astronomical Center, Poland
[23] SRON Netherlands Institute for Space Research, The Netherlands
[24] Sterrewacht Leiden, The Netherlands
[25] Deutsches Zentrum für Luft- und Raumfahrt e. V., Raumfahrt-Agentur, Bonn, Germany
[26] Department of Physics and Astronomy, University of Waterloo, Canada
[27] Osservatorio Astrofisico di Arcetri-INAF- Florence, Italy